NANO · MICRO small
www.small-journal.com

Catalytic Potential of Supported Superatoms

*Mehmet Emin Kilic and Puru Jena**

The importance of catalysts in industrial products is a driving factor in the search of efficient and cost-effective catalysts, creating considerable interest in the past decade in single-atom catalysis. One of the first requirements of a good catalyst is that it should bind to the molecules with energies intermediate between physisorption and chemisorption while simultaneously activating them. Herein, it is shown that superatoms, which are atomic clusters with fixed size and composition, can meet this challenge even better than the atoms whose chemistry they mimic. The reactions of molecules such as H_2, O_2, N_2, CO, NO, and CO_2 with an atom (Li) and its corresponding superatom (Li_3O) are confirmed through study. As these clusters need to be supported on a substrate for practical applications, the study focuses on the reaction of CO_2 with Li and Li_3O supported on graphene, Au(111), and Cu(111) substrates. Using density functional theory, it is shown that the Li_3O superatom can activate CO_2 far greater than the Li atom – stretching the CO bond from 1.16 Å to as large as 1.30 Å and bending the O—C—O bond angle from 180° to as low as 120°. Equally interesting, the results are not very sensitive to the substrate.

1. Introduction

Catalysts account for nearly 90% of the industrial chemicals produced in the world today. During the past year alone, the global catalyst market size was about USD 36.8 billion and growing. As most of the catalysts use expensive metals, there is considerable interest in developing efficient and cost-effective catalysts made of earth-abundant elements. In the past decade, there has been considerable interest in single-atom catalysts (SAC) where single atoms supported on a well-defined substrate play a fundamental role in heterogeneous catalysis.[1,2] Single-atom catalysts (SACs) have earned a reputation as the most promising advancement in the field However, they come with certain limitations. For example, having only one isolated atom can lead to insufficient adsorption sites, especially in reactions requiring the co-adsorption of multiple reactants. A common approach to address this issue is to introduce another isolated atom to create dual active sites, resulting in dual-atom catalysts (DACs).[3–5] Research indicates that DACs outperform SACs in CO_2 conversion.[6,7] However, there are no clear and systematic rules to select these DACs.

Here, we propose a new form of catalysts we term as single-superatom catalysts (SSAC). Superatoms[8–10] are clusters of atoms with specific size and composition that mimic the chemistry of atoms in the periodic table, even though they may not contain a single atom whose properties they mimic. Proposed in 1992,[8] considerable research in recent years has established rules[10] for the design and synthesis of the superatoms mimicking the chemistry of halogens, alkalis, chalcogens, and transition metal atoms.[11–13] In addition, superatoms have been used as building blocks of novel materials with applications in metal ion batteries, moisture-resistant solar cells, and materials exhibiting multiferroicity, thermoelectricity, and piezoelectricity.[14]

To provide proof of concept for SSACs, we note that two of the fundamental requirements every catalyst must possess are that they bind to molecules with energies intermediate between physisorption and chemisorption and activate them in the process. In this paper, we carried out a comprehensive study of the potential of a superatom capable of activating molecules far stronger than the atom whose chemistry it mimics, not just in the gas phase but, more importantly, when it is supported on a substrate. We focused on a well-known superatom, Li_3O, which mimics the chemistry of the Li atom. In early 1980′s, Gutsev and Boldyrev showed that the properties of Li_3O are superior to that of the Li atom.[15] They noted that like the Li atom, Li_3O has one more electron than needed for electron shell closure. As this electron in Li_3O is distributed over the entire cluster, its ionization potential would be smaller than that of the Li atom and they termed this cluster as a superalkali. Indeed, the measured ionization potential of Li_3O, namely, 3.59 eV[16] is much smaller than that of the Li atom, namely, 5.39 eV.[17] Since then, much work, both experimental and theoretical, have led to the discovery of many superalkalis[18] and superhalogens[19] that not only mimic the chemistry of alkali and halogen atoms, respectively, but surpass their properties with ionization potentials smaller than those of alkali atoms and electron affinities larger than those of halogen atoms. These superatoms, when used as the building blocks of materials yield novel solar cells, solid-state electrolytes in Li, Na,

M. E. Kilic, P. Jena
Department of Physics
Virginia Commonwealth University
Richmond, VA 23284-2000, USA
E-mail: pjena@vcu.edu

The ORCID identification number(s) for the author(s) of this article can be found under https://doi.org/10.1002/smll.202403888

DOI: 10.1002/smll.202403888

and Mg-ion batteries, thermoelectric materials with high figure of merit, and unconventional ferroelectric materials.[14]

Using spin-polarized Density Functional Theory (DFT) calculations, we first studied the interaction of isolated Li and Li_3O interacting with molecules such as H_2, O_2, N_2, NO, CO, and CO_2 and confirmed that Li_3O superatom mimics the chemistry of the Li atom and activates these molecules similar to the Li atom. However, when supported on graphene, Au(111) and Cu(111) substrates, Li_3O superatom outperforms the properties of the Li atom when interacting with a CO_2 molecule; the CO bond is stretched from 1.16 Å to as large as 1.30 Å and the O—C—O bond angle is reduced from 180° to as low a value as 120°. Equally important, the ability of the superatom to activate CO_2 is nearly independent of the substrate used. In the following, we outline the theoretical methods used and discuss the results of the interaction of molecules with isolated as well as supported Li and Li_3O.

2. Results and Discussion

Li_3O is a planar cluster with C_{3v} symmetry where the O atom occupies the centroid of a triangle formed by the three Li atoms (see Figure S1, Supporting Information). Its calculated ionization potential of 3.85–3.88 eV compares well with previous theoretical values[20,21] as well as the experimental value of 3.59 eV,[16] within the typical error associated with DFT methods. In comparison, the calculated ionization potential of the Li atom is larger, namely, 5.61–5.63 eV and is also consistent with the theoretical (5.3–5.7 eV)[22] and experimental value of 5.39 eV[17] (see Table S1, Supporting Information, for additional details). The HOMO-LUMO gap of Li_3O, namely, 1.21 eV is significantly smaller than that of the Li atom, namely, 3.07 eV.

2.1. Interaction of Isolated Li and Li_3O with H_2, O_2, N_2, NO, CO, and CO_2

H_2 was found not to bind to either the Li atom or the Li_3O superatom in the gas phase and hence is not discussed further. All other molecules are found to bind to both Li and Li_3O. The equilibrium geometries including bond lengths of O_2, N_2, NO, CO, and bond lengths and bond angles of CO_2 interacting with neutral Li and Li_3O are shown in **Figure 1**. In each case, the bond lengths of the isolated molecules are extended when interacting with both Li and Li_3O, with the bond lengths of the molecules interacting with Li_3O being marginally larger than that when interacting with the Li atom for the case of N_2, CO, and CO_2 (see **Table 1**). In particular, CO_2 is a linear molecule with the CO bond length of 1.169 Å and <O—C—O bond angle of 180° When interacting with Li and Li_3O, the CO bond length stretches to 1.254 Å and 1.262 Å, respectively while the <O—C—O bond angle significantly reduces to 128° in both cases. In Table 1, we present the binding energies (E_B), the total charge transfers (Δq) from Li and Li_3O to the molecules, and the bond length changes (ΔR) in O_2, N_2, NO, CO, and CO_2 molecules when interacting with an isolated single Li atom and Li_3O superatom in their respective equilibrium configurations. Note that, in every case, the molecules are more strongly bound to the Li_3O superatom than to the Li atom. This is because the ionization potential of Li_3O is smaller than that of the Li atom.

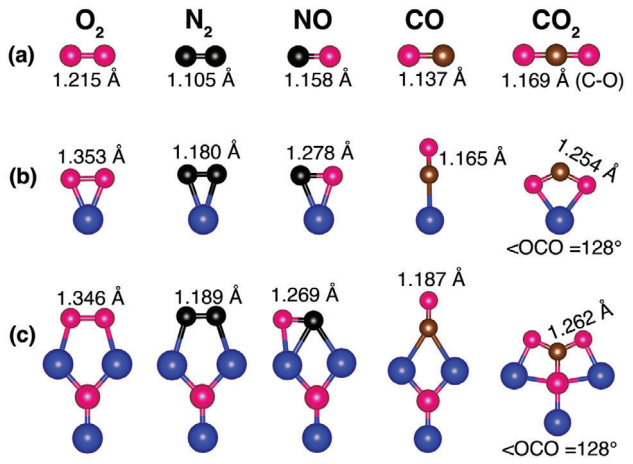

Figure 1. The equilibrium atomic configurations of a) free O_2, N_2, NO, CO, and CO_2 molecules, interacting with b) a single Li atom and c) Li_3O superatom. The bond lengths of the molecules before and after adsorption are given. Li, C, O, N atoms are in blue, brown, pink, and black colors, respectively.

Unlike in the case of a single atom where charge transfer exclusively takes place between the atom and the adsorbed molecule, a superatom offers multiple pathways for charge transfer. Here, all the atoms in it can take part. To examine the charge transfer between a single Li atom and the adsorbed molecule as well as that between a Li_3O superatom and the adsorbed molecule, we calculated the NBO charges. The results in Table 1 show that except for CO and CO_2, the charge transfer between the molecules and Li and Li_3O is rather similar. The stretching of the molecular bonds is also similar. These results confirm the expectation that the Li_3O superatom mimics the chemistry of the Li atom. The question that remains is whether this similarity persists when the atom and the superatom are supported on a substrate.

2.2. Structure and Bonding of Li and Li_3O Supported on Graphene, Au(111) and Cu(111) Substrates

As pointed out before, in practical applications, catalysts are supported on substrates. Thus, one must confirm that the supported superatom is still capable of binding molecules with energies intermediate between physisorption and chemisorption and

Table 1. Binding energies (E_B in eV) and total electron charge transfer (Δq) from Li and Li_3O to the molecules, and change in bond length (ΔR in Å) of molecules (O_2, N_2, NO, CO, and CO_2) when they are bound to either a single Li atom or a Li_3O superatom.

Adsorbed Molecules						
		O_2	N_2	NO	CO	CO_2
E_B	Li	2.53	0.06	1.69	0.14	0.84
	Li_3O	3.14	0.63	2.62	0.89	2.06
Δq	Li	0.91	0.82	0.92	0.49	0.91
	Li_3O	0.91	0.86	0.91	0.70	0.70
ΔR	Li	0.138	0.075	0.120	0.028	0.085
	Li_3O	0.131	0.084	0.111	0.050	0.093

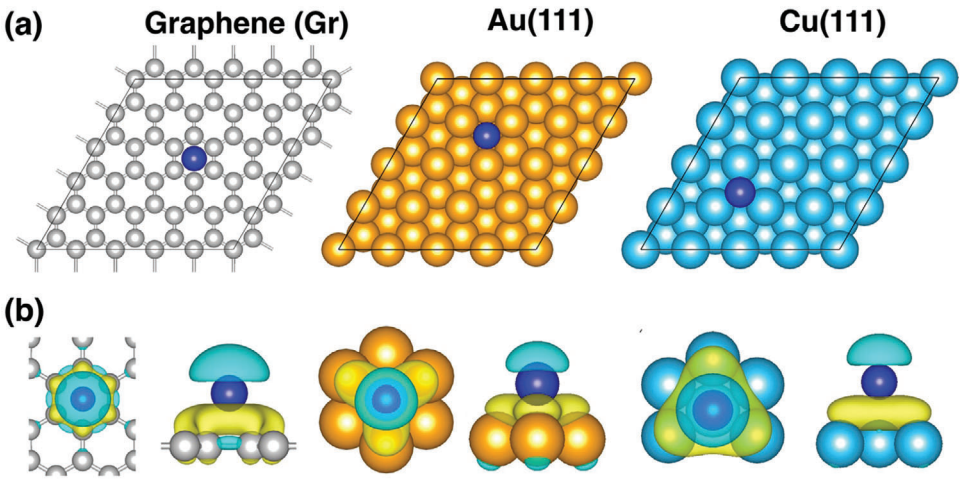

Figure 2. a) Energetically favorable position of a single Li atom on graphene, Au(111) and Cu(111) surfaces. Panel (b) displays the charge density difference before and after a single Li atom is adsorbed on these surfaces where yellow and cyan represent charge accumulation and depletion, respectively. C, Au, Cu, and Li atoms are represented by balls in gray, yellow, cyan, and blue colors, respectively.

simultaneously activating them. To see if the supported superatom not only meets these requirements but also is superior to that of the single atom, we have focused on the interaction of CO_2 with Li and Li_3O supported on three different substrates; graphene, Au(111) and Cu(111). It is expected that the geometry and the properties of a superatom may be modified once it interacts with the substrate atoms. In addition, the atoms on the surface may also relax. What is even more important to know is whether these changes help or hinder the above requirements.

The reason for our focusing on the interaction of CO_2 is that its capture and conversion are important to mitigate effects of climate change. Note that all the three substrates feature hexagonal arrangement of atoms, but their metallicity is different. Our objective is to see if the reaction of CO_2 with Li and Li_3O differs from that in the gas phase discussed above and if so, does it depend upon the substrate on which they are deposited.

In **Figure** 2a we present the lowest energy configurations of Li on graphene, Au(111) and Cu(111) surfaces. Top and side views of charge density difference where yellow and cyan regions show the accumulation and depletion of charge, respectively, are given in Figure 2b. The Li atom is found to occupy the hollow site in all cases and is bound to the graphene, Au(111) and Cu(111) substrates. In **Table** 2, we list the binding energies of the Li atom and the amount of charge transfer to the three substrates. From the charge density difference, illustrated in Figure 2b, we find that charge is transferred from the adsorbed Li atom to the corresponding substrates (see Figure 2b). According to the Bader charge analysis, the magnitude of the charge transfer in each of these cases remains nearly the same.

Table 2. Binding energies (in eV) and total charge transfer (in elementary charge, e) resulting from the adsorption of Li and Li_3O on graphene, Au(111) and Cu(111) surfaces. The charges of each lithium and oxygen atom within Li_3O superatom are presented in parentheses with positive and negative signs indicating electron gain and loss, respectively.

		Substrates		
		Graphene	Au(111)	Cu(111)
E_B	Li	1.30 eV	2.96 eV	2.65 eV
	Li_3O	1.91 eV	4.69 eV	4.76 eV
Δq	Li	−0.88 e	−0.88 e	−0.86 e
	Li_3O	−0.98 e	−1.21 e	−1.12 e

The equilibrium geometries of Li_3O deposited on the three substrates are shown in **Figure** 3a. The Li_3O geometry remains nearly unchanged from that in its gas phase. The oxygen atom is located at the hollow site on graphene and at the on-top site on Au(111) and Cu(111) surfaces. No distortion is observed in the surface morphology. The charge density differences depicted in Figure 3b reveal electron loss from Li atoms, while the oxygen atom in Li_3O, along with the three substrates, gain electron. Each Li atom loses 0.87, 0.86, and 0.85 electrons, and the oxygen atom gains 1.63, 1.37, and 1.43 electrons. Regarding the total charge transfer, Li_3O loses 0.98, 1.21, and 1.12 electrons when bound to graphene, Au(111), and Cu(111) substrates, respectively, surpassing the charge transfer observed in Li atom supported on the same substrates.

One can attribute this difference to the smaller ionization potential of Li_3O compared to that of the Li atom. This reflects on the binding energy of Li_3O to the substrate which is calculated as the energy difference between the substrate with Li_3O and the sum of the energy of the substrate and Li_3O. These are 1.91, 4.69, and 4.76 eV on graphene, Au(111), and Cu(111), respectively. Note that the binding energies of Li_3O supported on Au(111) and Cu(111) are significantly higher than those for the supported Li atom.

2.3. Activation of CO_2 Molecule with Li and Li_3O Supported Graphene, Au(111) and Cu(111) Substrates

To understand the activation of the CO_2 molecule, we analyzed the changes in the structure (specifically bond lengths and bond angle) and electronic properties (including molecular orbitals) upon gaining an additional electron (forming in a bent CO_2^-

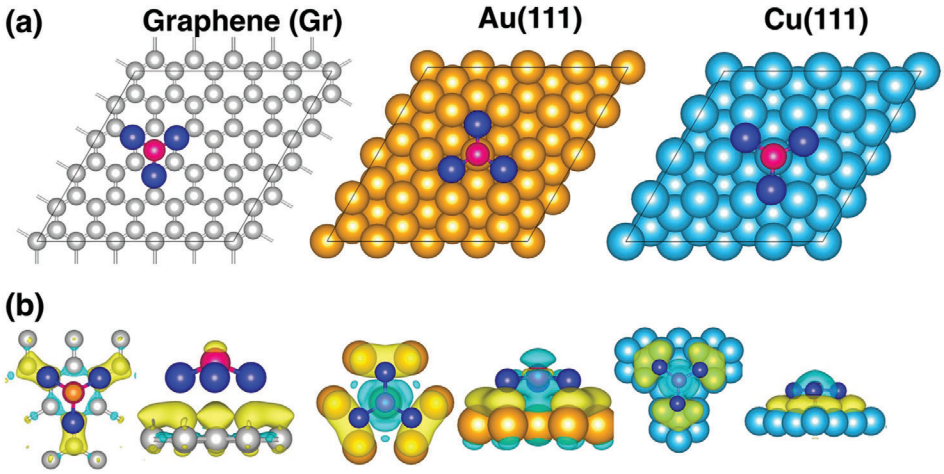

Figure 3. Energetically favorable position of a Li_3O superatom on graphene, Au(111) and Cu(111) surfaces. Panel (b) displays the charge density difference before and after a Li_3O superatom adsorbed on these surfaces where yellow and cyan represents charge accumulation and depletion, respectively. C, Au, Cu, Li, and O atoms are represented by balls in gray, yellow, cyan, blue, and pink colors, respectively.

configuration). The results are presented in **Figure 4**. It can be seen that the CO_2 molecule possesses a linear structure characterized by a delocalized π-type electron configuration. The highest occupied molecular orbital (HOMO) of CO_2 exhibits a non-bonding characteristic and involves 2p atomic orbitals around the two oxygen atoms. Below the HOMO energy (HOMO-1), there is a delocalized π-type bonding orbital. The LUMO is the σ-type anti-bonding orbital with main contribution from the C atom. Above the LUMO energy (LUMO+1), there are π-type anti bonding orbitals involving contributions from both the carbon and oxygen atoms. Therefore, it can be summarized that the activation of CO_2 molecule could occur in two possible ways: (i) CO_2 is activated by adding electrons into its lowest unoccupied molecular orbital (LUMO) and/or (ii) The lone pair electrons from the HOMO of CO_2 molecule are transferred to the active site. The energy level associated with the lone pair electrons is calculated as −10.47 eV, making it challenging to transfer electrons from the deep level to the active site. In contrast, the energy levels of σ^* (−0.56 eV) and π^* (0.35 eV) suggest that the predominant mode of activation in most cases is of the first type. This is confirmed by the molecular orbital of CO_2. When one extra electron is added, the C—O bonds elongate from 1.169 to 1.239 Å and the molecule bends with the O—C—O angle of 137°. This leads to substantial lowering of the 2p orbital, making it possible to accept electrons from the HOMO of the catalyst.

Next, we study the interaction of CO_2 with Li and Li_3O supported on graphene (Gr), Au(111), and Cu(111). The equilibrium geometries of CO_2 bound to the Li atom supported on the three

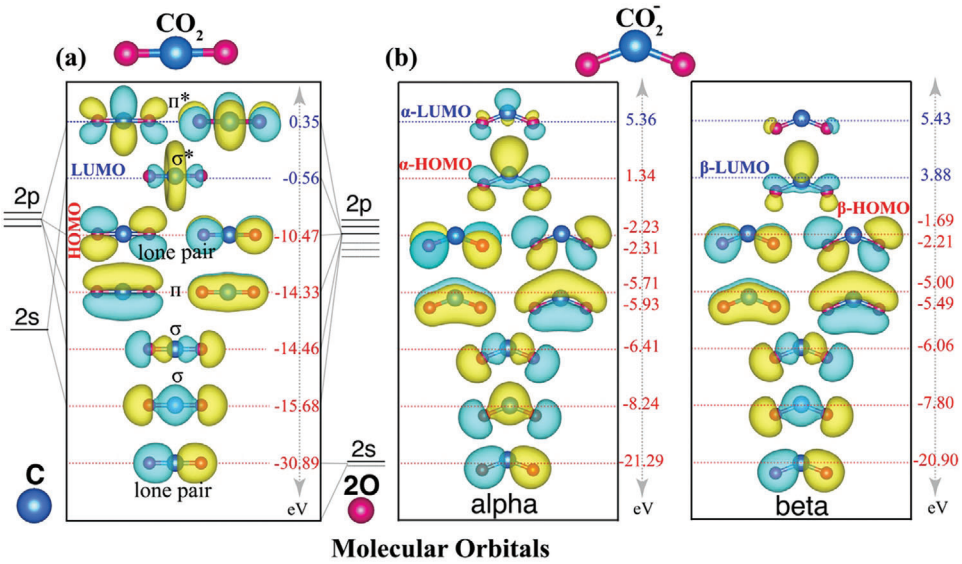

Figure 4. Molecular orbitals (MO) of (a) a free CO_2 molecule and b) its monoanion (CO_2^-). Yellow and cyan colors represent positive and negative charges, respectively.

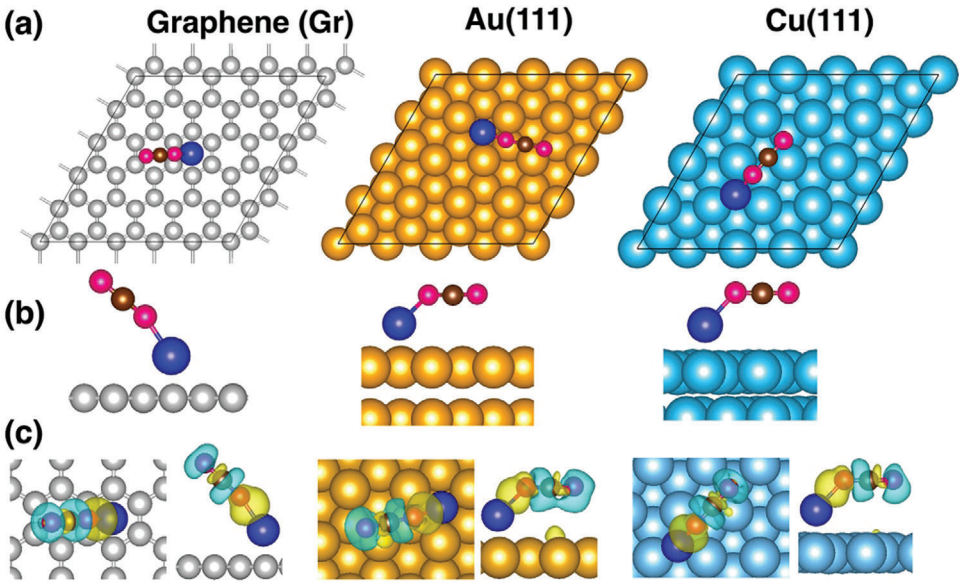

Figure 5. a) Top and b) side views of the lowest energy configuration of a CO_2 molecule bound to preabsorbed Li atom on graphene, Au(111) and Cu(111). Panel (c) displays the charge density difference before and after the CO_2 molecule is adsorbed on Li and Li_3O where yellow and cyan represent charge accumulation and depletion, respectively. C of graphene, C of CO_2 molecule, Au, Cu, Li, and O atoms are represented by balls in gray, brown, yellow, cyan, blue, and pink colors, respectively.

substrates are shown in **Figure 5**. In all cases, the CO_2 molecule remains nearly linear with O—C—O bond angles of 179°, 177°, and 177° on graphene, Au(111) and Cu(111), respectively. There are two different C—O bond lengths, namely C—O* (where O* refers to the oxygen atom bonded to Li) and C—O within the CO_2 adsorbed on the Li supported Gr, Au, and Cu. The results are summarized in **Table 3**. The C—O* bond (1.19 Å) is slightly elongated when compared to the C—O bond (1.17 Å) in the adsorbed CO_2 molecule on Li supported Gr, Au, and Cu surfaces. Thus, no notable activation of the CO_2 molecule is observed. Importantly, these results are very different from those when isolated Li atom interacts with CO_2 where the molecule was activated. The binding energies of CO_2 bound to the supported Li atom and Li_3O superatom and the corresponding charge transfer to the CO_2 molecule are given in Table 3. Note that the binding energies of CO_2 attached to the Li atom supported on graphene, Au(111) and Cu(111), namely, 0.48, 0.54, and 0.52 eV, respectively are rather weak.

Table 3. Binding energies (E_B, in eV), charge transfer (Δq in e) from/to CO_2 when adsorbed on supported Li and Li_3O. Positive and negative Δq values indicate electron gain and loss within the CO_2 molecule, respectively. Additionally, the <OCO bond angle (in degrees), the C—O*/C—O bond lengths (where O* refers to the oxygen atom bonded to Li), and the ICOHP values for the C—O* and C—O bond lengths upon CO_2 adsorption on the Li and Li_3O supported graphene, Au, and Cu surfaces.

		Substrates		
		Graphene	Au(111)	Cu(111)
E_B	Li	0.48	0.54	0.52
	Li_3O	1.86	1.31	1.84
Δq	Li	−0.01	+0.03	+0.05
	Li_3O	+0.39	+0.37	+0.49
<OCO	Li	179	177	177
	Li_3O	129	129	120
d(C—O*/C—O)	Li	1.181/1.167	1.187/1.165	1.186/1.166
	Li_3O	1.271	1.267	1.304
$ICHOP^{CO*/CO}$	Li	−9.72/−9.92	−8.18/−8.63	−8.14/−8.62
	Li_3O	−7.20/−7.23	−4.88/−4.88	−5.03/−5.02

According to the Bader charge analysis, there is nearly zero total charge transfer observed when a CO_2 molecule binds to the adsorbed Li atom on graphene, Au(111), and Cu(111) surfaces. These results align with the charge density difference depicted in Figure 5c, where charge accumulations and depletions are primarily localized between carbon and oxygen atoms of the adsorbed CO_2 molecule. Both the Bader charge and the charge density difference analysis indicate no significant charge transfer from/to the adsorbed Li atom on the corresponding substrates.

In **Figure 6**, we show the equilibrium geometries of CO_2 interacting with Li_3O superatom supported on graphene, Au(111) and Cu(111) substrates. Here, the results are very different from those of the supported Li atom. On both graphene and Au(111) substrates, the CO bond length is stretched to 1.27 Å while the <O—C—O bond angle is reduced to 129°. These results are similar to the interaction of CO_2 with isolated Li_3O superatom. Interaction of CO_2 with Li_3O supported on Cu(111), however, is again very different from that of graphene and Au(111). The Li_3O geometry breaks, and its O atom combines with CO_2 to form a planar structure leading to an equilateral triangle of CO_3. The CO bonds are further stretched to 1.31 Å and the <O—C—O bond angle is reduced to 120°. A structure where the Li_3O geometry is similar to that on graphene and Au(111) surface (see Figure S3, Supporting Information) is 1.34 eV higher than the ground state in Figure 5. The binding energies of CO_2 to Li_3O

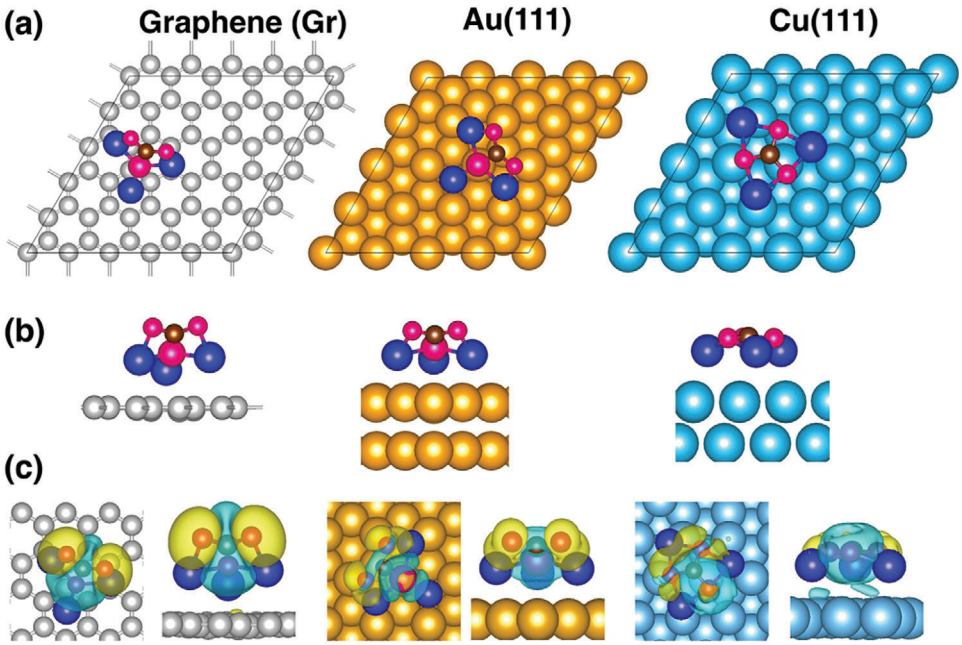

Figure 6. a) Top and b) side views of the lowest energy configuration of a CO_2 molecule bound to the pre-absorbed Li_3O superatom on graphene, Au(111), and Cu(111). Panel (c) displays the charge density difference before and after the CO_2 molecule is adsorbed on the surfaces where yellow and cyan represent charge accumulation and depletion, respectively. C, Au, Cu, Li, and O atoms are represented by balls in gray, yellow, cyan, blue, and pink colors, respectively.

supported graphene, Au(111) and Cu(111) substrates are 1.86, 1.31, and 1.84 eV, respectively. These binding energies are in the ideal range between physisorption and chemisorption. However, as the CO_2 combines with the oxygen atom in Li_3O to form CO_3 in Li_3O supported on Cu(111), in this case, the active sites may be blocked, restricting subsequent reactions.

According to the Bader charge analysis, upon adsorption, CO_2 bound to Li_3O supported on graphene, Au(111), and Cu(111) gains more electrons compared to Li supported on the same surface, by 0.39, 0.37, and 0.49 electrons, respectively. Figure 6c illustrates that charge accumulations primarily occur on Li-O bonds in Li_3O, whereas charge depletions are mainly localized on the C atom.

We additionally analyze the bonding and antibonding interactions in the adsorbed CO_2 molecule through Crystal Orbital Hamilton Population (COHP) analysis. The results are presented in **Figure 7** and Table 3. Positive -COHP value indicates bonding interactions while negative -COHP value indicates anti-bonding interaction. By integrating the COHP, we obtain the integrated COHP value (ICOHP), which yields the bonding strength between the two atoms. As one oxygen atom (referred to O*) of the adsorbed CO_2 binds to the Li supported on Gr, Au, and Cu surfaces, we evaluated COHP for C—O* and C—O bonds, depicted in orange and black in Figure 7, respectively. The results reveal that the $ICOHP^{C-O^*}$ value is slightly lower than the value of $ICOHP^{C-O}$. Thus, the strength of C—O* bonds is lower than that of C—O in the adsorbed CO_2 molecule on the Li supported on Gr, Au, and Cu surfaces. For instance, for the CO_2 adsorbed on the Li supported on Au surface, the $ICOHP^{C-O^*}$ and $ICOHP^{C-O}$ are found to be −8.18 and −8.63, which are slightly lower than the ICOHP of C—O bonds in the CO_2 gas phase ($ICOHP^{C-O}$ = −9.16), indicating that CO_2 is very little activated on the Li supported on surfaces. However, for the Li_3O supported on surfaces, the ICOHP values of the C—O bonds are almost half of those on the Li supported on surfaces. For instance, for the CO_2 adsorbed on Li_3O supported on Au surface, the $ICOHP^{C-O^*}$ value is −4.88. This indicates a significant weakening of the C—O bonds within the CO_2 molecule upon adsorption on the Li_3O supported surfaces. Therefore, the bending of the linear CO_2 molecule, elongation of the C—O bonds, and thereby the weakening of the C—O bond strength by the Li_3O superatom indicate the potential of superatoms to activate molecules, even the typical strong linear CO_2 molecule.

To further understand the significant activation of CO_2 molecule on superatoms, we calculated the spin-polarized and atom-projected density-of-states (PDOS). The PDOS results for the CO_2 adsorbed on the Li (Li_3O) supported on Gr, Au, and Cu surfaces are presented in Figure 7. On the Li supported surfaces, the PDOS of the CO_2 molecule shows two prominent peaks. However, the PDOS of the CO_2 molecule adsorbed on Li_3O supported surfaces reveals multiple peaks near Fermi energy. Remarkably, there is significant overlap in the PDOS between CO_2 molecule and Li_3O superatom. This suggests that there are many energy states that can be shared between them, and thus, indicates the strong interaction, and activation.

So far, our analysis has clearly demonstrated that superatoms outperform the single atoms in activating molecules, a crucial step in catalytic reactions. Moving forward, we investigate a simple catalytic process, namely hydrogen evolution reaction (HER). To determine the most stable hydrogen binding site for hydrogen on Li (Li_3O) supported on graphene, Au, and Cu surfaces, we placed a single hydrogen atom on the symmetric sites of

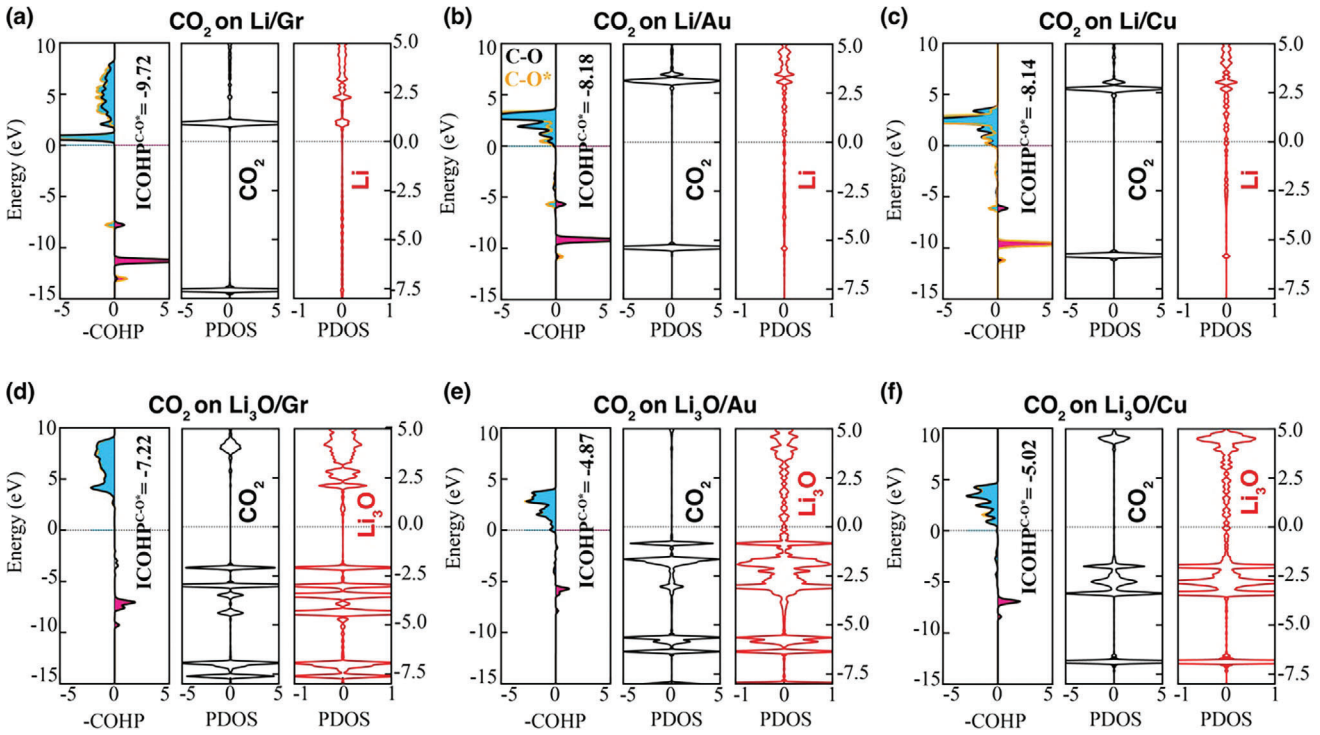

Figure 7. COHP analysis of CO bonds in CO_2 molecule adsorbed on Li (Li_3O) supported on graphene, Au, and Cu surfaces. Positive and negative COHP values indicate bonding and antibonding states, represented by pink and blue shading, respectively. Moreover, spin-polarized and atom-projected density-of-states (PDOS) for the CO_2 molecule and Li (Li_3O) on these surfaces are plotted in black and red, respectively.

these surfaces. All the calculated energies are given in Table S2 (Supporting Information). The results indicate that the hydrogen atom prefers to adsorb on top of the Li atom in Li supported graphene while it binds to the oxygen atom in the Li_3O supported-graphene. We calculated the Gibbs free energy changes for the Li (Li_3O) supported on graphene as 0.86 (0.07) eV. Remarkably, the free energy change in the Li_3O supported graphene is close to zero, indicating its potential for facilitating HER reactions. We did not study HER on Li_3O supported on Au(111) and Cu(111) surfaces as the H atom prefers to bind to the Au and Cu atoms, respectively, instead of the Li atom and the Li_3O superatom.

3. Conclusion

We explored the potential of a superatom in activating molecules more effectively than the atom whose chemistry it mimics. To demonstrate this concept, we chose Li atom and its corresponding Li_3O superatom as these are simple and well-studied systems. Interaction of a wide range of molecules (H_2, O_2, N_2, CO, NO, and CO_2) with isolated Li and Li_3O did confirm that the Li_3O superatom mimics the chemistry of the Li atom. However, the properties change when they are supported on a substrate. The studies were carried out by depositing Li and Li_3O on three substrates; graphene, Au(111), and Cu(111), and focusing their interaction with the CO_2 molecule. Interaction of CO_2 with the supported Li atom is rather weak and the CO_2 molecule remains mostly inactivated. However, the results are very different in the case of supported Li_3O superatom. Irrespective of the substrate, the CO_2 molecule undergoes strong activation, characterized by weakening of the CO bonds, elongation of the CO bond lengths, and significant reduction in the <OCO bond angle. We provided clear evidence of how superatoms activate molecules strongly, utilizing Bader charges, PDOS, and COHP analysis. The Gibbs free energy change for the HER on the Li_3O superatom supported on graphene is close zero, indicating its potential for promoting catalytic reactions compared to that of the supported Li atom.

Note that the field of superatom is rather rich and numerous superatoms have been found that mimic the chemistry of halogens, chalcogens, pnictogens, as well as transition and rare earth metals.[14] We hope that this study will motivate both theoretical and experimental work to study the interaction of superatoms with molecules both in isolated and supported configurations. To assess the full potential of the superatoms supported on well-defined substrates as a new class of single-superatom catalysts, further work is needed as reaction pathways and energy barriers have to be analyzed for each process. We hope that this study will stimulate such studies – both theoretically and experimentally.

4. Computational Methods

All calculations are carried out using the Density Functional Theory (DFT). The geometries and corresponding total energies of isolated Li and Li_3O cluster interacting with various molecules (H_2, O_2, N_2, NO, CO, and CO_2) in the gas phase are calculated using the Gaussian-16 code[23] with the B3LYP exchange-correlation functional[24,25] and the 631G+(d,p) and def2-tzvp basis sets. For the study of Li and Li_3O supported on graphene, Au(111), and Cu(111) substrates and their interaction with the CO_2 molecule,

we used the periodic boundary condition and spin polarized DFT implemented in the Vienna Ab initio Simulation Package (VASP) code.[26,27] The ion-electron interactions are modeled using the projector-augmented wave formalism (PAW)[28] and the Perdew-Burke-Enzerhof (PBE)[29] formulation of the exchange-correlation functional. To account for the long-range dispersion forces, we used the (DFT+D3) approach by Grimme.[30] A plane-wave basis set with cutoff energy of 520 eV and the Brillouin zone (BZ) integration with a 4 × 4 × 1 k-point Γ-centered mesh are used in all calculations. The atomic positions are optimized using a conjugate-gradient (CG) algorithm without any symmetry constraint. The convergence of the total energy and force components on each atom are set to 1×10^{-5} eV and 0.01 eV $Å^{-1}$, respectively.

To determine the preferred site of a single Li atom and Li_3O superatom on the graphene, Au (111), and Cu (111) substrates and the adsorption of the CO_2 molecules, it is essential to construct sufficiently large enough supercell where the spurious interactions between the images are small. In the case of graphene, we created a 5 × 5 supercell containing 50 carbon atoms, and introduced an additional 20 Å of vacuum space normal to the graphene plane. For Au and Cu, a 4 × 4 supercell of the (111) plane was created using periodic slabs, with a vacuum region exceeding 15 Å between vertically repeated slabs. We also employed a perpendicular dipole correction to enhance energy convergence of the adsorbed systems. The model for Au(111) and Cu(111) slabs consisted of four atomic layers, where the bottom two layers were frozen to the theoretical equilibrium bulk position of Au and Cu, while the two uppermost layers, namely surface layers, were free to relax during the optimization (see Figure S2a, Supporting Information). Justification for the use of a four atomic layer slab is given in the supporting information.

To evaluate the adsorption strength of molecules interacting with Li and Li_3O in the gas phase, the binding energy (E_B) was computed using the formula,

$$E_B = E(X) + E(Y) - E(XY) \quad (1)$$

where $E(X)$ denotes the total energy of either a single Li atom or a Li_3O superatom, $E(Y)$ represents the total energy of a molecule such as H_2, O_2, N_2, NO, CO, or CO_2, and $E(XY)$ represents the total energy of the Y molecule bound to X. The positive value of E_B indicates that Y binds to X.

To examine the bonding and antibonding interactions between pairs of atoms, we performed Crystal Orbital Hamilton Population (COHP) analysis using the LOBSTER program.[31,32]

To evaluate the HER performance of the Li single atom and its super atom Li_3O, we used the computational hydrogen electrode (CHE) model proposed by Norskov et al.,[33]

$$H^+(aq) + e^- \; 1/2H_2(g) \quad (2)$$

The change of free energy for the step $*X + H^+ + e^- \rightarrow *XH$ is determined by the reaction: $*X + 1/2H_2(g) \rightarrow *XH$ at 0 V versus the reversible hydrogen electrode (RHE) at all pH levels. The changes in the Gibbs free energy (ΔG_{H*}) were calculated as:

$$\Delta G_{H*} = \Delta E_{ads} + \Delta E_{ZPE} - T\Delta S \quad (3)$$

where ΔE_{ads} is the adsorption energy of hydrogen, ΔE_{ZPE} is the energy change in the zero-point energy. ΔS is the change in entropy at temperature T (T = 298.15 K).

The atomic charges were calculated using the Bader charge analysis as implemented by Henkelman and coworkers.[34] To examine the charge transfer between X and Y, we calculated charge density differences ($\Delta\rho$) by subtracting the individual electron densities, $\rho(X)$ and $\rho(Y)$, both calculated in the geometry of the combined system $\rho(XY)$, from the density of the total system across the volume of the supercell used,

$$\Delta\rho = \rho(XY) - \left[\rho(X) + \rho(y)\right] \quad (4)$$

The lowest energetic configurations of a single Li atom and a Li_3O superatom interacting with various molecules (H_2, O_2, N_2, NO, CO, and CO_2) was determined by varying the relative orientation between Li/Li_3O and the molecules. For the single atom in the gas phase, we initially positioned the molecule with two different orientations: parallel and perpendicular (Figure S2b, Supporting Information). Unlike a single atom, a superatom exhibits a significantly greater degree of freedom for the molecule to adsorb as it can bind to any one of the atoms in the superatomic cluster. Hence, for Li_3O in the gas phase, we initially placed the molecule on each site with different molecular orientations.

For Li/Li_3O supported on different substrates, we systematically examined energetically the most favorable positions of Li/Li_3O on high-symmetry sites of graphene, Au(111), and Cu(111) surfaces. Considering hollow (H), bridge (B), and on-top (T) sites for graphene, as well as hollow-fcc (H_F), hollow-hcp (H_H), B, and T sites for Au(111) and Cu(111) surfaces (see Figure S2c,d, Supporting Information), we initially placed the Li atom and the Li_3O superatom with different orientations on each of these sites. Next, total energies were calculated for all the considered configurations to determine the lowest energetic structure. Subsequently, we investigated the energetically preferred configurations of adsorbed molecules on pre-adsorbed Li/Li_3O on these surfaces. Likewise, we positioned the adsorbed molecule on these surface symmetric sites, both in proximity to and at a distance from the pre-adsorbed Li/Li_3O. The resulting lowest energetic configurations are subjected to further analysis.

Supporting Information

Supporting Information is available from the Wiley Online Library or from the author.

Acknowledgements

This work received partial support from the US Department of Energy, Office of Basic Energy Sciences, Division of Materials Sciences and Engineering, under Award No. DE-FG02-96ER45579. The authors also acknowledge the resources provided by the National Energy Research Scientific Computing (NERSC) Center, supported by the Office of Science of the US Department of Energy under Contract No. DE-AC02-05CH11231. The authors would like to express their gratitude to the High-Performance Research Computing (HPRC) core facility at Virginia Commonwealth University for granting access to supercomputing resources.

Conflict of Interest

The authors declare no conflict of interest.

Data Availability Statement

The data that support the findings of this study are available from the corresponding author upon reasonable request.

Keywords

single-superatom catalyst, single-atom catalyst, superalkali, super-atoms

Received: May 13, 2024
Revised: July 12, 2024
Published online:

[1] B. Qiao, A. Wang, X. Yang, L. F. Allard, Z. Jiang, Y. Cui, J. Liu, J. Li, T. Zhang, *Nat. Chem.* **2011**, *3*, 634.
[2] A. Wang, J. Li, T. Zhang, *Nat. Rev. Chem.* **2018**, *2*, 65.
[3] T. He, A. R. P. Santiago, Y. Kong, M. A. Ahsan, R. Luque, A. Du, H. Pan, *Small* **2022**, *18*, 2106091.
[4] L. Lei, X. Guo, X. Han, L. Fei, X. Guo, D. Wang, *Adv. Mater.* **2024**, 2311434.
[5] X. Wang, L. Xu, C. Li, C. Zhang, H. Yao, R. Xu, P. Cui, X. Zheng, M. Gu, J. Lee, H. Jiang, M. Huang, *Nat. Commun.* **2023**, *14*, 7210.
[6] S. Lu, M. Mazur, K. Guo, D. C. Stoian, M. Gu, W. M. Tucho, Z. Yu, *Small* **2024**, *20*, 2309251.
[7] Y. Shao, Q. Yuan, J. Zhou, *Small* **2023**, *19*, 2303446.
[8] S. N. Khanna, P. Jena, *Phys. Rev. Lett.* **1992**, *69*, 1664.
[9] P. Jena, *J. Phys. Chem. Lett.* **2013**, *4*, 1432.
[10] P. Jena, Q. Sun, *Chem. Rev.* **2018**, *118*, 5755.
[11] D. E. Bergeron, A. W. Castleman, T. Morisato, S. N. Khanna, *Science* **2004**, *304*, 84.
[12] D. E. Bergeron, P. J. Roach, A. W. Castleman, N. O. Jones, S. N. Khanna, *Science* **2005**, *307*, 231.
[13] S. Giri, B. Z. Child, P. Jena, *ChemPhysChem* **2014**, *15*, 2903.
[14] P. Jena, Q. Sun, *Superatoms: Principles, Synthesis and Applications*, John Wiley & Sons, Hoboken, NJ **2021**.
[15] G. L. Gutsev, A. I. Boldyrev, *Chem. Phys. Lett.* **1982**, *92*, 262.
[16] K. Yokoyama, H. Tanaka, H. Kudo, *J. Phys. Chem. A* **2001**, *105*, 4312.
[17] B. A. Bushaw, W. Nörtershäuser, G. W. F. Drake, H.-J. Kluge, *Phys Rev A* **2007**, *75*, 052503.
[18] W. Sun, D. Wu, *Chemistry* **2019**, *25*, 9568.
[19] P. Skurski, in *Superatoms*, Wiley, Hoboken, NJ **2021**, pp. 53–84.
[20] C. Paduani, A. M. Rappe, *J. Phys. Chem. A* **2016**, *120*, 6493.
[21] M. Gutowski, J. Simons, *J. Phys. Chem.* **1994**, *98*, 8326.
[22] R. D. Johnson, http://srdata.nist.gov/cccbdb **2006**.
[23] M. J. Frisch, G. W. Trucks, H. B. Schlegel, G. E. Scuseria, M. A. Robb, J. R. Cheeseman, G. Scalmani, V. Barone, G. A. Petersson, H. Nakatsuji, X. Li, M. Caricato, A. V. Marenich, J. Bloino, B. G. Janesko, R. Gomperts, B. Mennucci, H. P. Hratchian, J. V. Ortiz, A. F. Izmaylov, J. L. Sonnenberg, D. Williams-Young, F. Ding, F. Lipparini, F. Egidi, J. Goings, B. Peng, A. Petrone, T. Henderson, D. Ranasinghe et al., Gaussian 16 Revision C.01, **2016**.
[24] A. D. Becke, *J. Chem. Phys.* **1993**, *98*, 5648.
[25] C. Lee, W. Yang, R. G. Parr, *Phys. Rev. B* **1988**, *37*, 785.
[26] G. Kresse, D. Joubert, *Phys Rev B* **1999**, *59*, 1758.
[27] G. Kresse, J. Furthmüller, *Comput. Mater. Sci.* **1996**, *6*, 15.
[28] P. E. Blöchl, *Phys Rev B* **1994**, *50*, 17953.
[29] J. P. Perdew, K. Burke, M. Ernzerhof, *Phys. Rev. Lett.* **1996**, *77*, 3865.
[30] S. Grimme, J. Antony, S. Ehrlich, H. Krieg, *J. Chem. Phys.* **2010**, *132*, 154104.
[31] V. L. Deringer, A. L. Tchougréeff, R. Dronskowski, *J Phys Chem A* **2011**, *115*, 5461.
[32] S. Maintz, V. L. Deringer, A. L. Tchougréeff, R. Dronskowski, *J. Comput. Chem.* **2016**, *37*, 1030.
[33] J. K. Nørskov, J. Rossmeisl, A. Logadottir, L. Lindqvist, J. R. Kitchin, T. Bligaard, H. Jónsson, *J Phys Chem B* **2004**, *108*, 17886.
[34] G. Henkelman, A. Arnaldsson, H. Jónsson, *Comput. Mater. Sci.* **2006**, *36*, 354.